Surfaces and Interfaces 24 (2021) 101059

Contents lists available at ScienceDirect

Surfaces and Interfaces

journal homepage: www.sciencedirect.com/journal/surfaces-and-interfaces

Functions of 2-butyne-1,4-diol in the process of tin-silver alloy electrodeposition from the acidic sulfate solution

M.A. Shikun [a,*], O.N. Vrublevskaya [b], T.N. Vorobyova [a]

[a] Belarusian State University, Minsk, Belarus, 220006, Leningradskaya st., 14
[b] Research Institute for Physical Chemical Problems of the Belarusian State University, Minsk, Belarus, 220006, Leningradskaya st., 14

ARTICLE INFO

Keywords:
Tin-silver alloy
Electrodeposition
Eutectic
2-Butyne-1,4-diol
Cementation
Corrosion

ABSTRACT

The eutectic (at.%) Sn96,7/Ag3,3 alloy (T_{melt} 221 °C) is used for assembling electronic products and soldering jewelry. Control of the Sn-Ag alloy composition during its electrodeposition is a challenging task due to significant difference in electrode potentials of tin and silver and the tendency of Sn(II) to oxidation and hydrolysis. In this work the composition of known acidic sulfate electrolyte for electrochemical deposition of Sn–Ag alloy was modified by the addition of 2-butyne-1,4-diol (BD). The purpose was to study the effect of BD on simultaneous Sn(II) and Ag(I) electrochemical reduction, the nature of side processes which accompany the deposition of Sn–Ag coatings, their composition and structure. It is shown that the addition of BD to the electrolyte reduces silver content in Sn−Ag alloy and provides obtaining near-eutectic alloy according to its elemental, phase composition and melting temperature. The presence of SnO and SnO_2 oxides and the increased silver content in the near-surface zone of the coatings no more than 3 nm deep are distinctive features of the deposited Sn–Ag alloy coatings. These features are due to the occurrence of side processes of Ag(I) reduction with tin and the alloy corrosion, which accompany simultaneous Sn(II) and Ag(I) reduction. The BD additive in the electrolyte inhibit Ag(I) electroreduction, slightly accelerates Ag(I) cementation with freshly reduced tin, but retards corrosive dissolution of the alloy and hydrogen evolution.

1. Introduction

The eutectic (at.%) Sn96,7/Ag3,3 alloy (T_{melt} 221 °C) is used for electronic products assembling. In the form of rings, wires this alloy is produced metallurgically [1] or by mechanical treatment and subsequent melting of a mixture of Sn and Ag powders [2]. Powdery alloy can be synthesized by chemical reduction of Ag(I) and Sn(II) with the strong reducing agent, such as borohydride ions [3,4], as well as in the result of Ag(I) cementation with tin in solutions [5]. Tin-silver alloy coatings are obtained via layer-by-layer spraying, chemical or electrochemical deposition of tin and silver films with various thicknesses and their subsequent heat treatment for the alloying [6–8]. The acidic sulfate [9, 10] and methanesulfonic [11] electrolytes with pH ≤ 2 or alkaline pyrophosphate, pyrophosphate-iodide, pyrophosphate-cyanide [10,12–14] solutions with pH 8–11 are used for electrochemical deposition of Sn–Ag alloy coatings.

Electrochemical Sn–Ag alloy plating has a number of advantages such as obtaining coatings of the required thickness; not expensive equipment; low energy consumption; multiple use of solutions. However, the electrochemical synthesis of a tin–silver alloy with the controlled and relatively small silver quota is a challenging task. Difficulties are due to the dominance of silver in the alloy; a lack of the electrolyte stability owing to uncontrolled reduction of Ag(I) with Sn(II) and Sn(IV) hydrolysis [5,13]. The dominance of Ag(I) reduction processes is due to the large difference in standard electrode potentials of tin and silver, the values of which are $E^0(Sn^{2+}/Sn^0) = -0.136$ V and $E^0(Ag^+/Ag^0) = +0.799$ V. The variation of Sn(II) and Ag(I) concentration in real electrolytes in the absence of any ligands can only slightly affect this ratio. For example, a sharp diminishing of $AgNO_3$ concentration from 1.0 to 0.005 mol dm^{-3} lowers electrode potential only to +0.663 V. A more significant decrease in the value of the electrode potential of silver is possible by binding Ag(I) into complex compound with a high stability constant. In this case concentration of free silver(I) is lowered by many orders of magnitude and the convergence of both metals electrode potentials can be achieved.

It is important to point other ways providing the enrichment of the alloy with tin such as the subpotential reduction of tin(II); the addition of surfactants which being adsorbed at the cathode prevent charge transfer [15,16].

* Corresponding author.
E-mail addresses: marina.shikun21@gmail.com (M.A. Shikun), vrublevskaya@bsu.by (O.N. Vrublevskaya), vorobyovatn@bsu.by (T.N. Vorobyova).

https://doi.org/10.1016/j.surfin.2021.101059
Received 12 October 2020; Received in revised form 25 February 2021; Accepted 26 February 2021
Available online 2 March 2021

Thiourea (Tu) or cyanide ions are introduced into the sulfate or pyrophosphate-cyanide Sn–Ag plating electrolytes to form stable Ag(I) complex compounds. Stability constants of $Ag[Tu]_2^+$, $Ag[Tu]_3^+$ [17] and $Ag(CN)_2^-$ are of $1.6 \cdot 10^{11}$, $2.5 \cdot 10^{13}$ and $7.1 \cdot 10^{19}$, respectively. In some cases supplementary ligands such as thiocyanate ions [12] and EDTA [14]) are used to form mixed complex compounds with Ag(I).

A number of other problems connected with chemical properties of Sn(II) should be noted. Electrochemical reduction of tin(II) from aqueous solutions is complicated by Sn(II) oxidation to Sn(IV) with the dissolved oxygen, the anodic oxidation of Sn(II), the hydrolysis of Sn(II) and Sn(IV) compounds. Formed as a result of hydrolysis oxy- and hydroxy- compounds adsorb on the surface of coatings and change their properties, especially solderability [18]. Tin(II) oxidation can be partially suppressed by the addition of inhibitors, such as quinones, phenolsulfonic acid, naphtholsulfonic acid, hydrazine, pyrogallol, etc. [16]. The hydrolysis of tin(II) compounds is significantly slowed down in strongly acidic solutions [18].

A number of additives are introduced into electrolytes for Sn-Ag alloy deposition such as PEG [13], gelatin [19], S-dodecylmercaptobenzimidazole [20] and etc. They fulfill different functions including the diffusion and absorption control of metal ions reduction thereby facilitating the deposition of uniform, fine-grained and compact coatings. Gelatin is an unstable additive, S-dodecylmercaptobenzimidazole is toxic.

2-Butyne-1,4-diol (BD) seems to be the most promising for several reasons. The first of them is based on the results of the work [21] which show that the "BD adsorption on the electrode surface moderately hinders silver(I) transfer from the solution bulk to the outer boundary of the electrode double layer and affects the electrocrystallization stage". The second reason is based on the data of the work [22] which testify to the formation of stable Cu(I) π-complexes with BD. That allowed us to assume the similar complexation ability of silver which, like copper, belongs to the elements of 1B group. The third reason is the fact of the BD stability during the electrolyte operation and the fact that it is not involved in electrochemical cathodic or anodic processes in a wide range of potentials, as it was shown in [21] and was testified in our experimental work presented below. The fourth reason is based on our previous results on the development of an electrolyte for deposition of tin-silver alloy with the composition close to the eutectic which is applicable for microassembly of electronic products [23]. In the mentioned work it was shown that the BD additive decreased silver content in the alloy. The reasons of the BD specified action are not known.

The purpose of this work was to study the effect of BD on the peculiarities of Sn(II) and Ag(I) simultaneous and single electrochemical reduction from the sulfuric bath containing Tu and catechol. The data presented in this manuscript characterize Sn-Ag alloy phase and elemental composition dependently on the BD concentration in the electrolyte, chemical composition of the alloy at different depth of coatings; their morphology; thermal behavior of the alloy; side processes accompanying the electrochemical deposition of the Sn-Ag alloy.

2. Experimental details

Sn–Ag alloy coatings were electrodeposited from the solution referred in [9,10], which was modified with catechol as anti-oxidant and BD ($C_4H_4(OH)_2$). The solution (SA) used in this experiment contained 0.1 mol $SnSO_4$, 0.005 mol $AgNO_3$, 0.053 mol $SC(NH_2)_2$ (Tu), 0.005 mol $C_6H_6O_2$ (catechol), 0.005–0.05 mol BD in 1 dm^3 of water. The pH value was of 0.5. Sn-Ag coatings were deposited at direct current density (j) of 8 mA cm^{-2} and the temperature of 20 ± 2 °C without the solution stirring. Electrode/cell geometry is shown in Figure S1, a. At a higher j the formation of dendrites occurred which was noticeably suppressed in the presence of BD. A decrease in current density to the values of 5 mA cm^{-2} or less caused a slowdown in the growth of coatings when BD was added to the electrolyte.

The ratio of cathodic and anodic areas was 1 : 16. In case of galvanostatic electrodeposition of the alloy, two platinum plates (99.9 wt.%) were used as anodes, located symmetrically on both sides at the same distance (5 cm) from the cathode (see Fig. S1, a). Copper foil covered with Ni−P coating was used as the cathode. Ni−P underlayer not less than 1.5 μm thick was used to avoid the diffusion of tin into the copper.

The thickness of coatings and the rate of their deposition were determined by gravimetric method with the sensitivity of $5 \cdot 10^{-5}$ g. The root mean square error was not more than 4%. The thickness, l (μm) and current efficiency (CE) were calculated according to the Faraday's law taking into account the weight of the coating, its surface area, the quotas of tin and silver in the alloy, and their densities.

Silver and tin content in the coatings was analyzed by energy dispersive X-ray microanalysis (EDX) using Rontec attachment to LEO-1420 microscope. The morphology of coatings was studied with the usage of scanning electron microscope LEO 1420.

Chemical composition of Sn−Ag alloy coatings and the depth distribution of the elements in them were monitored by X-ray photoelectron spectroscopy (XPS). The measurements were performed using JPS – 3030 spectrometer equipped with X-ray non monochromatic AlK_α source working at 12 kV and 25 mA. Energy resolution for the survey spectrum equaled to 1.8 eV, the pass energy and energy step were 50 eV and 1 eV respectively. The analyzed area was about 6 mm^2. Argon etching was performed to study the composition of coatings at their different depth. Acceleration voltage of Ar^+ was 500 V. The etching was performed at a rate of 30 nm min^{-1} related to SiO_2.

X-ray diffraction (XRD) analysis was performed with X-ray diffractometer DRON-3 (Russia) using CuK_α radiation. JCPDS card files were used for phase identification.

Thermal behavior of the Sn–Ag alloy within the temperature range of 30–400 °C was studied using the method of synchronous thermal analysis (NETZSCH STA 449 Jupiter, Germany). Differential scanning calorimetry (DSC) curves were recorded at the rate of temperature raise 10 K min^{-1} in the atmosphere of 99.9% nitrogen.

Electrochemical investigations (cyclic voltammetry (CV), electrochemical impedance spectroscopy (EIS), corrosion analysis) were conducted with PGstatAutolab controlled by Nova 2.1 software in standard cell for electrochemical investigations (Fig. S1, b) using platinum counter and Ag/AgCl reference electrodes. The working electrodes were graphite rod [24,25] or copper foil covered with Ni–P, Sn, Ag, and Sn−Ag alloy coatings. CV curves were recorded at a rate of potential sweep of 20 mV s^{-1}. Graphite rod was used as the working inert electrode. It had a grade of spectral purity. The working surface was a section perpendicular to the axis of the rod. The walls of graphite rod were hermetically sealed with polymer material stable in the acid media which excluded the possibility of electrolyte contact with the walls of the electrode. Before each experiment, the graphite rod was carefully prepared. The working surface was ground off to a depth of about 5 mm to remove the impurities adsorbed during previous experiments. Then this surface was polished to a mirror finish, washed and dried. The open circuit potential of graphite electrode did not change for half an hour or more.

Before each measurement copper foil covered with Ni–P, Sn, Ag, and Sn−Ag alloy was treated in 5% HCl and washed in distilled water. The electrochemical cell was deaerated with Ar before each impedance measurement.

3. Results and discussion

3.1. Sn-Ag alloy coating composition

Gravimetric analysis has shown that regardless of the BD presence in the SA electrolyte the rate of Sn–Ag coating deposition at current density of 8 mA cm^{-2} is 10.8 ± 0.4 μm h^{-1}.

It was determined that the quota of silver in coatings 1 − 5 μm thick, deposited in the absence of BD, equals to 14.1–15.3 at.% (Fig. 1, a). The

addition of the BD to the solution in concentration 0.005 mol dm^{-3} causes a decrease in silver content in coatings by 1.6 times. Thus, this content reaches 9.1–9.4 at.%. Further increase in the BD concentration has little effect on the ratio of tin and silver in coatings. Thus, the rise of the BD concentration to 0.5 mol dm^{-3} causes the diminution of the silver content in the alloy to 7.1–8.1 at.%. The CE of Ag(I) reduction is about 10−20 times lower as compared with Sn(II) reduction (Fig. 1, b). The addition of BD enhances this difference. CE of tin(II) reduction in the solution without BD is 65 ± 3%, BD addition cause the increase in CE by 1.3 times reaching 83 ± 3%. CE of silver decreases from 7.6% to 4.5 ± 0.4%.The total CE of both metals does not reach 100% due to the simultaneous reduction of hydrogen(I) at the cathode. In the BD absence the total CE does not exceed 73%.

It is important to note that the SA electrolyte with the BD additive is stable for 3–4 months and during this period the deposited alloy coatings do not change their composition.

XPS method was used to examine the composition of coatings on their surface and in their bulk. Sn-Ag coatings 1.5 μm thick with silver quota of 9.1 at.%, according to EDX data, were deposited from the SA solution containing 0.015 mol dm^{-3} of BD. Fig. 2 and 3 demonstrate survey XPS spectrum of the surface and high-resolution O1s, $Ag3d_{5/2}$, $Sn3d_{5/2}$, $S2p_{3/2}$ region spectra of Sn-Ag coatings recorded at different duration of Ar etching till the depth of 1.5 μm.

XPS spectra in Fig. 2 and 3 together with the depth profile of different atoms distribution in the subsurface layer 10 nm thick (Fig. 4) indicate the presence of silver, tin, oxygen and trace quantity of carbon atoms on the surface of Sn−Ag coatings.

The depth composition profiles of coatings (Fig. 3, a, d) indicate that oxygen atoms are present only on the surface and in a narrow near-surface zone of the coatings. Tin atoms dominate both on the surface and in the bulk of the coatings, although the near-surface layer is strongly enriched in these atoms. The quota of silver is extremely small in the depth of the coatings, but its content in a narrow near-surface zone is higher.

For the top layer of Ag–Sn coating Sn3d spectrum exhibited spin-orbit doublet peaks at 495.2 ($3d_{3/2}$) and 487.3 eV ($3d_{5/2}$) (Fig 3, c). The procedure of decomposition of XPS $Sn3d_{5/2}$ line shows three types of tin bonding, that are Sn^{2+} (486.7 eV, for SnO 486.0–486.8 eV [26,27]), Sn^{4+} (487 eV, for SnO_2 486.4–486.9 eV [26,27]), Sn^0 (485 eV [26,27]) (Fig S2, a). These data coincide with the results presented in [28] describing Sn–Ag alloy obtained via layer-by-layer electrochemical deposition with subsequent heat treatment at 373 K. Handbook data for the value of binging energy $Sn3d_{5/2}$ in metal tin is 485 eV [26]. The discovered binding energy shift for $Sn3d_{5/2}$ by 0.7 eV is attributed to tin in its alloy with silver [27]. Chemical state of tin in Sn−Ag coating at the depth of 2 nm changes (Table 1). Judging by the intensity and shape of

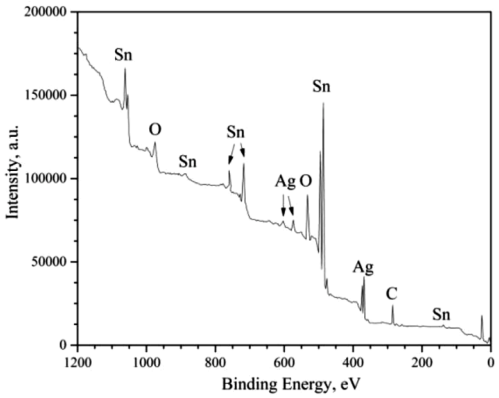

Fig. 2. Survey XPS spectrum of the surface of Sn−Ag coating.

Sn $3d_{5/2}$ region spectra the quota of tin oxides sharply diminishes, and metal tin becomes dominant as its quota equals to 83.6 at.%.

XPS O1s spectrum is presented by a broad and asymmetrical band with clear maximum at 531 eV (Fig. 3, a) which is broadened to the side of smaller energies. The decomposition of this band makes it possible to identify oxygen bound to tin in two oxidation states (Fig S2, b), that are 530.5 eV ($O–Sn^{+4}$), 529.8 eV ($O–Sn^{+2}$) [27,28]. At further etching of the coating oxygen disappears in spectra. This is consistent with the data on the decrease in tin oxides content (see Table 1) and indicates the absence of tin oxides in the alloy bulk.

XPS Ag3d spectrum presented in Fig. 3, b shows the bands at 374.8 $Ag3d_{3/2}$ and 368.5 eV$Ag3d_{5/2}$ that are close to binding energies of 374.9 and 368.2 eV in metal silver, the shift in binding energy is observed as a result of the alloying of silver with tin [26,29].

Depth-composition profiles of the elements distribution in Sn–Ag coating 1.5 μm thick with total silver content of 9.1 at.% are presented in Fig. 4. Silver distribution in the coating is non-uniform. The quota of silver on the coating surface is about 10 at.% and it increases up to 58 at.% at the depth of 2 nm. At a depth > 2 nm silver quantity decreases sharply: there is 7 at.% of silver at a depth 6 nm. XPS data show that the coating surface is contaminated with carbon compounds which are not included into the alloy composition and disappear at the etching with argon. Owing to the availability of these contaminations the relative content of silver on the coating surface is somewhat underestimated.

The fact of too large silver content equal to 58 at.% at the depth of 2 nm deserves an explanation, because it substantially exceeds the integral silver percentage in the coating. The increased silver content can be caused by proceeding of Ag(I) cementation with the electrochemically reduced tin according to the reaction:

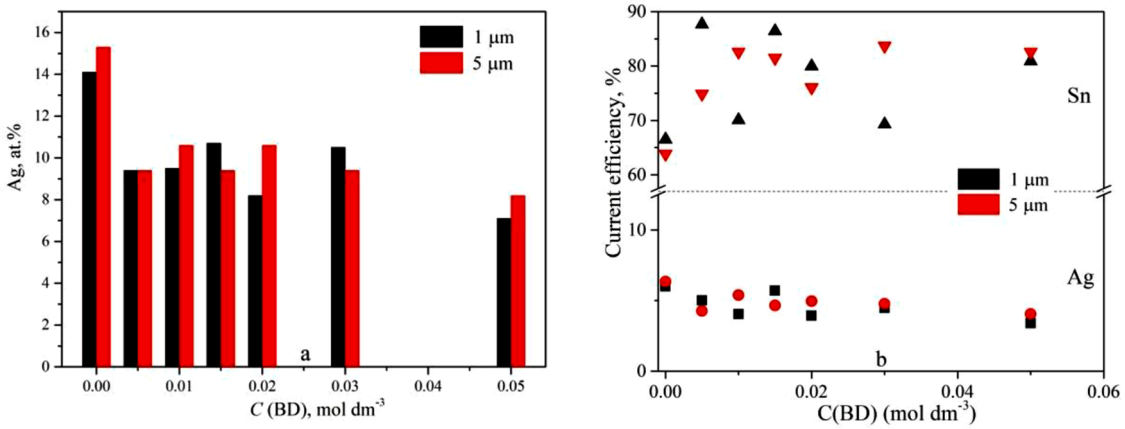

Fig. 1. The dependence of silver quota (a) in Sn−Ag coatings 1−5 μm thick and CE (b) of Ag(I) and Sn(II) reduction at Sn-Ag alloy deposition on the BD concentration in the SA solution (mean square error – 5%).

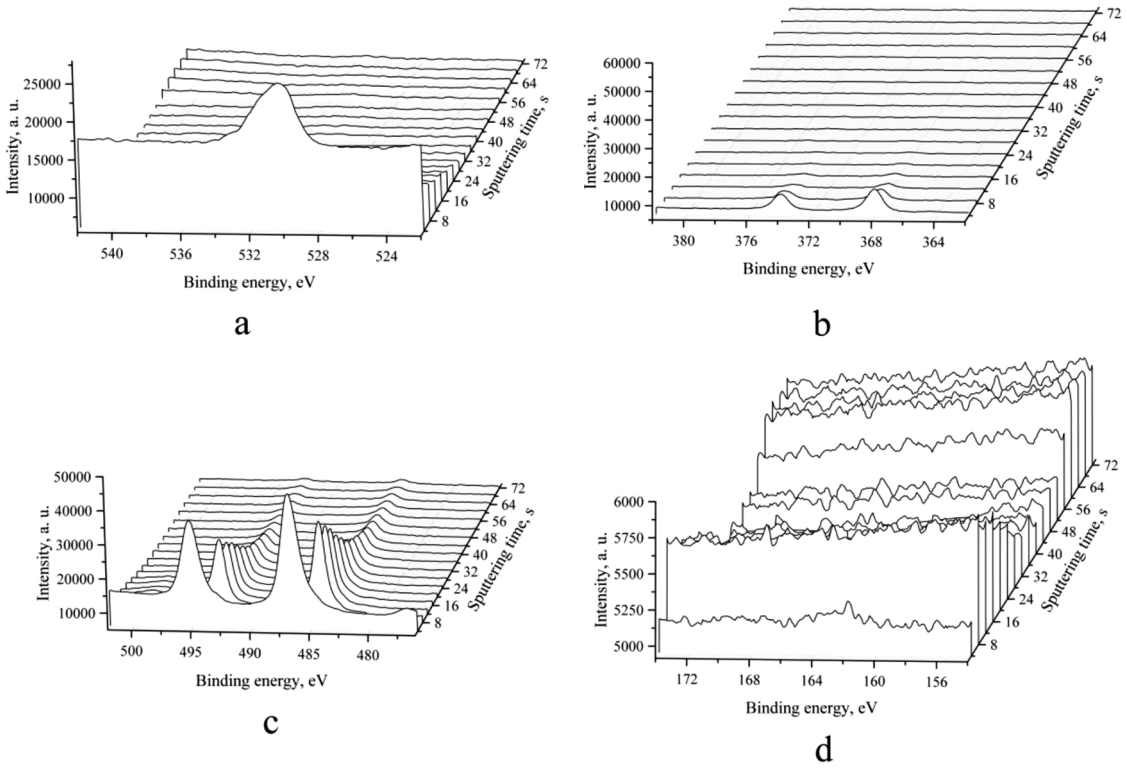

Fig. 3. 3D transformation of XPS spectra in the depth of Sn-Ag coating at the etching with argon: (a) – O1s, (b) – Ag3d, (c) – Sn 3d, (d) – S2p, Sn-Ag coating thickness is 1,5 μm.

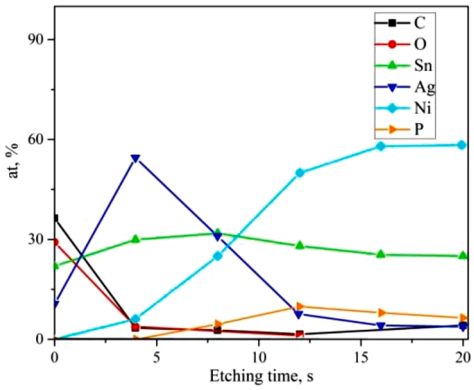

Fig. 4. Depth profile of Sn–Ag coating in its near surface zone up to the depth of 10 nm.

Table 1
Quotas of tin in different chemical state in Sn−Ag coating before and after the etching with argon.

Etching time, s	Sn^0 Quota, at.%*	SnO	SnO_2
0	6.9	1.7	91.4
4 (depth 2 nm)	83.6	6.9	9.4

* Quota was calculated from the quantity of tin atoms in different oxidation state.

$$Sn^0 + 2Ag^+ \rightarrow Sn^{2+} + 2Ag^0. \quad (1)$$

Proceeding of this reaction was revealed earlier. The authors of the work [5] have found that Ag(I) cementation with tin plate proceeded with the rate of 1.5 μm h^{-1} in the solution similar to that used in this work. This value is 7 times smaller than the value of the rate of electrochemical Sn−Ag coating deposition. Thus, the process of electrochemical reduction dominates and determines silver quota in the bulk of the coating.

Depth profile (Fig. 4) shows the availability of nickel in Sn–Ag coating already at the depth of 2 nm that indicates the porosity of the alloy coating. Since nickel sublayer was obtained by Ni(II) reduction with hypophosphite ions the samples contain small amount of phosphorus.

XPS analysis of Sn–Ag coating deposited in the absence of the BD in the electrolyte gives the similar results except for a significantly higher quota of silver in the samples under study.

According to XRD study Sn−Ag coatings include crystalline phases of metallic β-Sn and Ag_3Sn intermetallic compound (Fig. 5, a). Tin oxides are not detected because according to XPS data they are located in a thin surface layer of the coating 2–3 nm thick. Consequently, their quantity and the layer thickness are too small to be detected by X-ray phase analysis.

It should be added that Sn-Ag coatings deposited in the absence of BD contain a greater amount of silver, up to 15% or more. Nevertheless, the crystalline phase of silver also was not found in them. They include only two crystalline phases which are β-Sn and Ag_3Sn. It means that all the reduced silver is included only into the intermetallic compound.

DSC curves of the alloy coating containing silver in the quantity of 14.1–15.3 at.% of silver show one endothermal peak at 221 °C that gives evidence on the composition of Sn−Ag coating the same with the eutectic one (Fig. 5, b). The DSC curves recorded for coatings deposited in the absence of BD and containing silver in the quantity 14.1–15.3 at.% have endothermal peak at 227 °C which is shifted to the melting point of tin. It is broader and not so intensive.

Judging by the increased silver quota in the near-surface layer of Sn-Ag coating and inclusion of all silver into Ag_3Sn intermetallic compound, we conclude that there is an abundance of Ag_3Sn in the near-

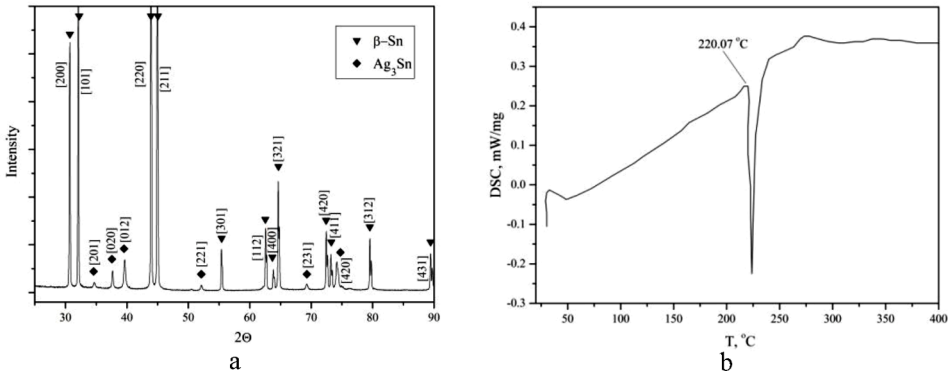

Fig. 5. XRD pattern (a) and DSC-curve for Sn-Ag coating with silver content of 7.1–9.4 at.%.

surface zone about 2−3 nm thick. In deeper layers of coatings the quota of intermetallics is constant.

3.2. Morphology of Sn-Ag coatings

SEM study of Sn–Ag coatings morphology indicated that in the absence of the BD in the electrolyte, there are two types of particles on the coatings surface (Fig. 6, a). Particles of one type are well-faceted crystals in the form of square plates, cubes, and parallelepipeds 0.5–2.0 μm in size fused with each other. Particles of another type are much smaller, 0.1–0.2 μm in size, rounded and more contrast. These small particles are located on the surface of larger crystals in the amount from several to 10 particles per crystal. They can belong to intermetallic phase. Possibly, they contain silver reduced in the result of the cementation (reaction 1). Earlier it was shown [5] that the formation of intermetallic compound occurs in the process of Ag(I) cementation with tin.

Sn–Ag coatings 1.5 μm thick obtained in the absence of the BD are rather porous (Fig. 6, a). The sizes of pores range from 0.2 to 2.0 μm and their concentration is 30 pores per 100 μm^2. The porosity of coatings explains the fact of nickel availability in XPS spectra of Sn–Ag coatings (Fig. 4).

The morphology of Sn–Ag coatings deposited from the electrolyte containing the BD additive in concentration of 0.005 mol dm^{-3} is rather different. This is expressed in the formation of crystals with less distinct shape, which are more closely fused with each other. The most important difference is the lower concentration and size of small contrast particles, and especially the lower concentration of large pores (Fig. 6, b).

As the BD concentration is increased to 0.015 mol dm^{-3}, the morphology of the coatings continues to change. Due to strong fusion of crystals with each other, it becomes difficult to determine their shape and size (Fig. 6, c). An important difference between coatings is the small size and concentration of pores in the latter case. The sizes of pores

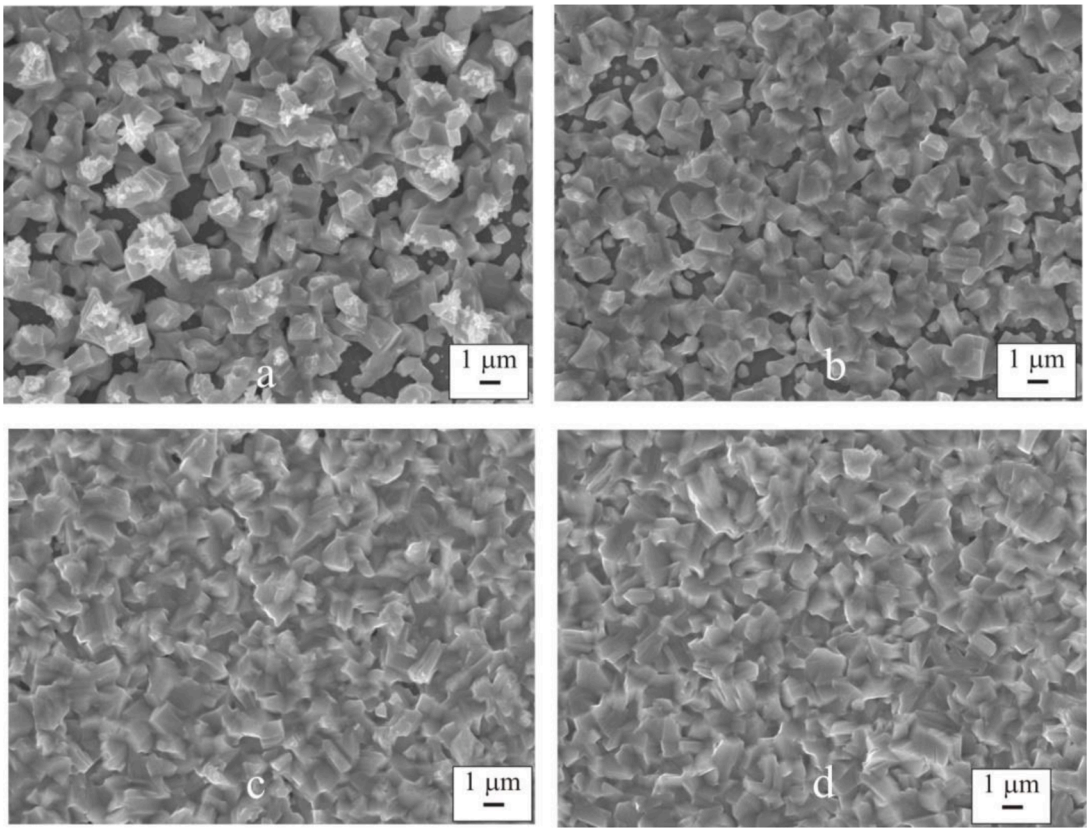

Fig. 6. SEM images of Sn–Ag coatings 1.5 μm thick deposited from the SA solution containing BD, mol dm^{-3}: (a) – 0, (b) – 0.005, (c) –0.015, (d) – 0.050.

are decreased to 0.1–0.6 μm, and their number is diminished to 8 pores per 100 μm^2.

With further increase in the BD concentration to 0.05 mol dm^{-3} the surface morphology of coatings does not change (Fig. 6, d).

Thus, the introduction of the BD into the SA solution affects the structure of the alloy. Coatings become less porous, the grains constituting the coating are denser packed.

3.3. Redox processes occurring on electrodes in a solution for electrochemical deposition of Sn–Ag alloy

According to CV curves presented in Fig. 7, a, the hydrogen evolution (region I) on graphite electrode in the background solution occurs at the potentials less than −0.70 V:

$$H_3O^+ + 2\,e^- \rightarrow H_2 + OH^-. \quad (2)$$

At the addition of the BD into background electrolyte region I is shifted by 30 mV to the side of more negative values, and the hydrogen evolution proceeds with the diminished cathodic current.

Anodic current at +(0.20–0.50) V was registered because of oxygen evolution (region II, Fig. 7, a):

$$2H_2O - 4\,e^- \rightarrow 4H^+ + O_2. \quad (3)$$

BD does not have any influence on this process.

Very small cathodic current (region III, Fig 7, a) was observed in the potentials range of −(0.40–0.70) V regardless of the BD availability. It can be attributed to the reduction of oxygen absorbed on the surface of graphite electrode according to the reaction:

$$O_2 + 4e^- + 4H^+ \rightarrow 2H_2O. \quad (4)$$

In the absence of Sn(II) and BD the reduction of Ag(I), (region IV, Fig. 7, b), begins at −0.28 V and slowly proceeds at a potential sweep to −0.47 V according to the reaction:

$$Ag^+ + e^- \rightarrow Ag^0. \quad (5)$$

A plateau of diffusion limiting current of 0.05 mA cm^{-2} appears at −(0.47–0.53) V owing to very small concentration of Ag(I) in the electrolyte. The dependence of cathodic peak current on square root of the scan rate is linear (Fig. S3). So the Ag(I) reduction is diffusion-limited one. In the region of more negative potentials the current of hydrogen evolution is observed. In the presence of BD in concentration of 0.015 mol dm^{-3} the value of limiting current is slightly lower and amounts to 0.03 mA cm^{-2}.

The reduction of Sn(II) in the absence of Ag(I) and BD begins at the potential of −0.47 V (region VI, Fig. 7, c) according to the reaction:

$$Sn^{2+} + 2e^- \rightarrow Sn^0. \quad (6)$$

The Sn(II) reduction and Sn(0) oxidation (region VII) peak-to-peak separation is larger than 28.5 mV (as for two-electron transfer reaction) and shifts with scan rate (Fig. S4). It means that Sn(II) reduction is

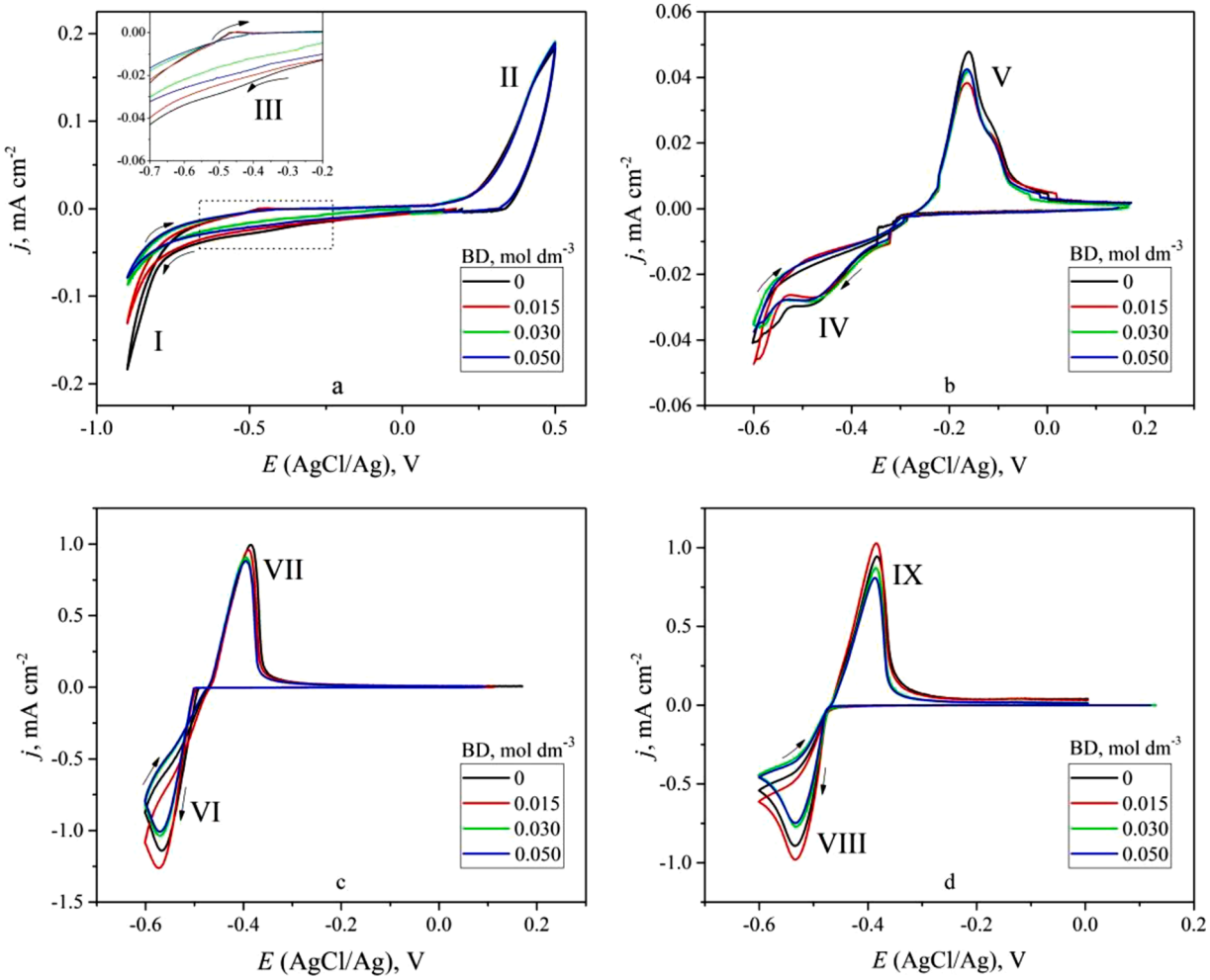

Fig. 7. CV curves demonstrating the behavior of graphite electrode in the background solution (a), electrolyte in the absence of Sn(II) (b), electrolyte in the absence of Ag(I) (c), in the SA electrolyte of complete composition (d).

electrochemically irreversible: electron transfer at the electrode surface is slow compared to mass transport [30]. Cathodic current rapidly increases with the potential sweep and at −0.53 V its value is approximately 30 times higher than the value of limiting current of Ag(I) reduction. In case of the BD presence in concentration of 0.015 mol dm^{-3}, the cathodic current of Sn(II) reduction is increased by 25%. Further twofold and more increase in the BD concentration on the contrary causes the decrease in the cathodic current of Sn(II) reduction.

Simultaneous reduction of Ag(I) and Sn(II) in the absence of the BD begins at a potential of −0.47 V which is the same as in case of Sn(II) reduction (region VII, Fig. 7, d). At a potential sweep to −0.53 V cathode current rises quickly up to 0.90 mA cm^{-2} that is slightly less than in case of individual Sn(II) reduction. The plateau of limiting current typical for Ag(I) reduction is absent. The slope of the cathodic branch of the CV curve indicates that in the absence of the BD Sn(II) is reduced with an insignificant overpolarization effect.

At the BD addition to the SA electrolyte the slope of cathodic branch of the CV curve increases and the effect of overpolarization of Sn(II) reduction disappears. An increase in the BD concentration to 0.03 mol dm^{-3} and more enhances the overpolarization effect of Sn(II) reduction.

Analysis of the anodic branches of the CV curves shows that the oxidation of silver (region V, Fig. 7, b; reaction 7), which is reduced during cathodic sweep of the potential, proceeds at potentials from −0.23 to −0.00 V, in contrast to the oxidation of tin (reaction 8) in the range from −0.47 to −0.33 V, regardless of the BD presence in the electrolyte (see Fig. 7, b, c; Table 2).

$$Ag^0 - e^- \rightarrow Ag^+ \quad (7)$$

$$Sn^0 - 2e^- \rightarrow Sn^{2+} \quad (8)$$

Sn–Ag alloy is oxidized (region IX, Fig. 7, d) at the same potential values as pure tin does (region VII, Fig. 7, c). This confirms the fact of low Ag_3Sn quotas in the alloy. The addition of the BD into the electrolyte causes a slight diminution of the anodic current inherent as for tin, so as for silver oxidation. In case of tin and silver co-deposition, the alloy formed oxidizes a little less intensively as compared with individual tin, judging by the density of the anodic currents. This may be due to the presence of Ag_3Sn intermetallic compound in the alloy.

To clarify the BD function in the SA solution the method of electrochemical impedance was used. Graphite rod was used as a working electrode. Nyquist plots for SA solution with varied BD concentration at open circuit potential are shown in Fig. 8, a.

There are two capacitive semicircles in Nyquist plot. The first semicircle (I, Fig. 8, a) corresponds to capacitive artifact originated in stray capacity of counter and reference electrodes. This is also confirmed by low phase angle in high frequency range ($\Theta < -90°$) (Fig. S5, a). This phenomenon limits impedance measurement only at high frequencies, it doesn't depend on solution resistance, and so impedance spectra can be analyzed in frequency range 10^5–10^{-2} Hz. [31,32].

Regardless of the BD concentration the impedance spectra have the same shape. Non-linear increment of semicircle radius means that capacitive and resistive elements parameters are changed with variation of the BD concentration. The impedance spectra were modeled with equivalent circuit presented in Fig. 8, b. Resistance R_1 and constant phase element CPE_1 are included as artifact elements and it will not be considered. R_2 element is the solution resistance; CPE_2 is the constant phase element characterizing double layer properties; R_3 is the charge transfer resistance. Constant phase element impedance can be written as [33]

$$Z_{CPE} = \frac{1}{Y_0(j\omega)^n}, \quad (9)$$

where Y_0 is admittance value, n is constant phase exponent related to the deviation of the straight capacitive line from 90° by the angle $\alpha = 90°(1 - n)$, ω is angular frequency.

The modeling showed that minimal solution resistance (34.8 Ω) corresponds to the solution with 0.015 mol dm^{-3} of BD (Table 3). The increase in the BD concentration leads to the solution resistance growth. Since calculated parameter $n_2 > 0.80$, CPE_2 can be considered as a capacitor with inhomogeneous surface and the effective capacitance (C_{eff}) of double layer can be calculated. The effective capacitance drops into 2.2 times in the presence of 0.015 mol dm^{-3} of BD and varies only slightly with the increase in the BD concentration. This phenomenon can be explained in two ways: (i) BD molecules or complex ions entering into double layer increase its thickness, i. e. the increase in the distance between theoretical capacitor plates; (ii) introduced species raise the conductivity of media between theoretical capacitor plates. Also the charge transfer resistance is minimal in the solution with 0.015 mol dm^{-3} of BD, but the resistance rises with increasing concentration. All electrochemical model impedance parameters are presented in Table S1.

It is important to emphasize that the decrease in grains sizes of Sn-Ag alloy in case of adding BD to the electrolyte, as well as the change in the calculated values of the effective capacitance of the theoretical capacitor, are similar to the results described in the work [21]. The authors of this article associated the revealed change in the surface morphology of silver coatings (grain sizes decrease, packing density) with the BD adsorption on the electrode surface.

The electrochemical impedance spectra at applied potential (AP) were obtained to evaluate the BD effect on separate Sn(II) and Ag(I) reduction. For such experiment the graphite electrode behavior in solutions without tin(II) (solution A) and silver(I) (solution S) was evaluated. The AP value was slightly more negative, than the potentials of Sn (II) and Ag(I) reduction in BD containing solutions (see Fig. 7, b, c).

Working electrode was kept in a cell at applied potential during 15 min before each measurement. Since the Ag(I) reduction process is diffusion-limited and the reaction rate is low the impedance spectra did not allow us to evaluate the BD influence on the process of interest. There are two capacitive semicircles in Nyquist plot for solution A at –0.320 V which are similar to previous case (inset in Fig. 9, a). The first one is the artifact reflection ($\Theta < -90°$) (Fig. S5, b). Since there are no any other effects, the second semicircle can characterize the solution-electrode interface. That is why the equivalent circuit at Fig. 8, b was used for modeling of the system. Electrochemical model impedance parameters from Bode plots of graphite electrode in solution A at –0.320 V are presented in Table S2.

Nyqiust plots for graphite electrode in solution S at applied potential of –0.495 V include three semicircles. Symmetric semicircles correspond to artifact (I) (in Bode plots (Fig. S5, c) $\Theta < -90°$) and double layer capacitance (II). The third skewed one (III) characterizes the electrochemical reduction of Sn(II) on the surface of the working electrode (or Sn(IV) reduction). This process was modeled well by Gerisher element connected in series with charge transfer resistance (Fig. 9, c).

The Gerisher impedance can be written as [34]

$$Z_G = \frac{1}{Y_0\sqrt{K_a + j\omega}}, \quad (10)$$

where K_a is electrochemical reaction constant.

Table 2
Analysis of the anode branches of the CV curves illustrating the behavior of the graphite electrode in the SA solution.

Reduced metal	Potential range of anodic dissolution, V	Potential of the peak of anodic dissolution, V	Maximal current density of anodic dissolution, BD is absent in the electrolyte, mA cm^{-2}	Maximal current density of anodic dissolution, BD is added to the electrolyte, mA cm^{-2}
Ag	−(0.23–0.00)	−0.16	0.05	0.04
Sn	−(0.47–0.33)	−0.38	0.90	1.00
Sn–Ag	−(0.47–0.33)	−0.38	1.00	0.95

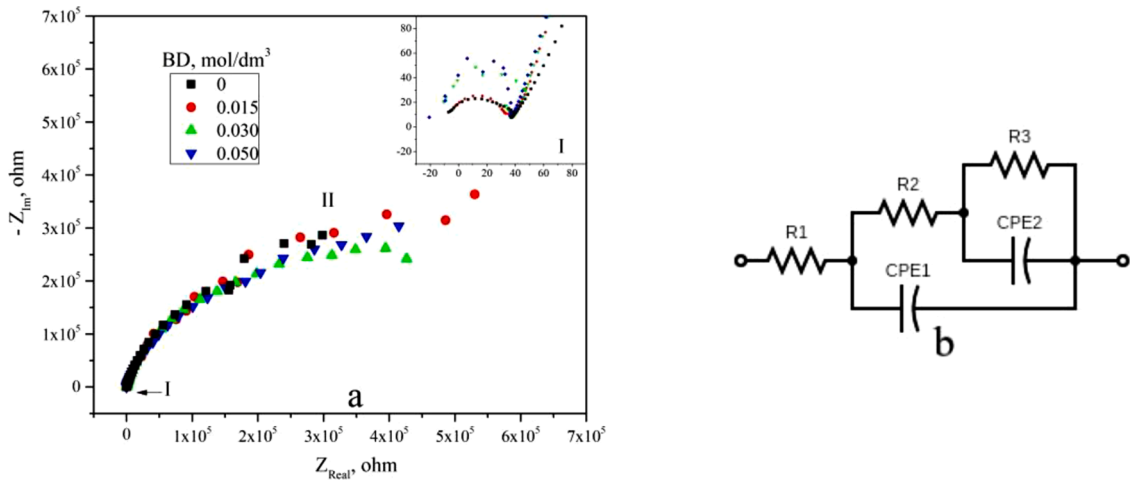

Fig. 8. Nyquist plots (a) for graphite electrode at open circuit potential in SA solution with different BD concentration, b – equivalent circuit proposed for modeling.

Table 3
Analyzed electrochemical model impedance parameters from Bode plots of graphite electrode in SA solution at open circuit potential.

BD concentration, mol dm^{-3}	0	0.015	0.030	0.050
R_2, Ω	39.0	34.8	38.5	36.2
R_3, Kω	754	555	613	643
$Y_{0,2}$, μS	13.9	8.29	8.02	8.80
n_2	0.814	0.843	0.843	0.831
C_{eff}, μF	23.8	11.0	10.8	12.5

Calculated solution S resistance is minimal (41.1 Ω) when 0.015 mol dm^{-3} of BD is added (Table 4). There are an increase in n_2 parameter and non-linear decrease of charge transfer resistance with BD concentration increasing. It is worth noting that the reaction constant calculated from Gerisher element is the highest for the solution with 0.015 mol dm^{-3} of BD. Since the cell was deaerated with Ar before each experiment to limit the possibility of Sn(IV) formation, most likely this reaction constant describes the reduction of Sn(II). All electrochemical model impedance parameters are presented in Table S3.

Results of electrochemical experiments showed that the addition of

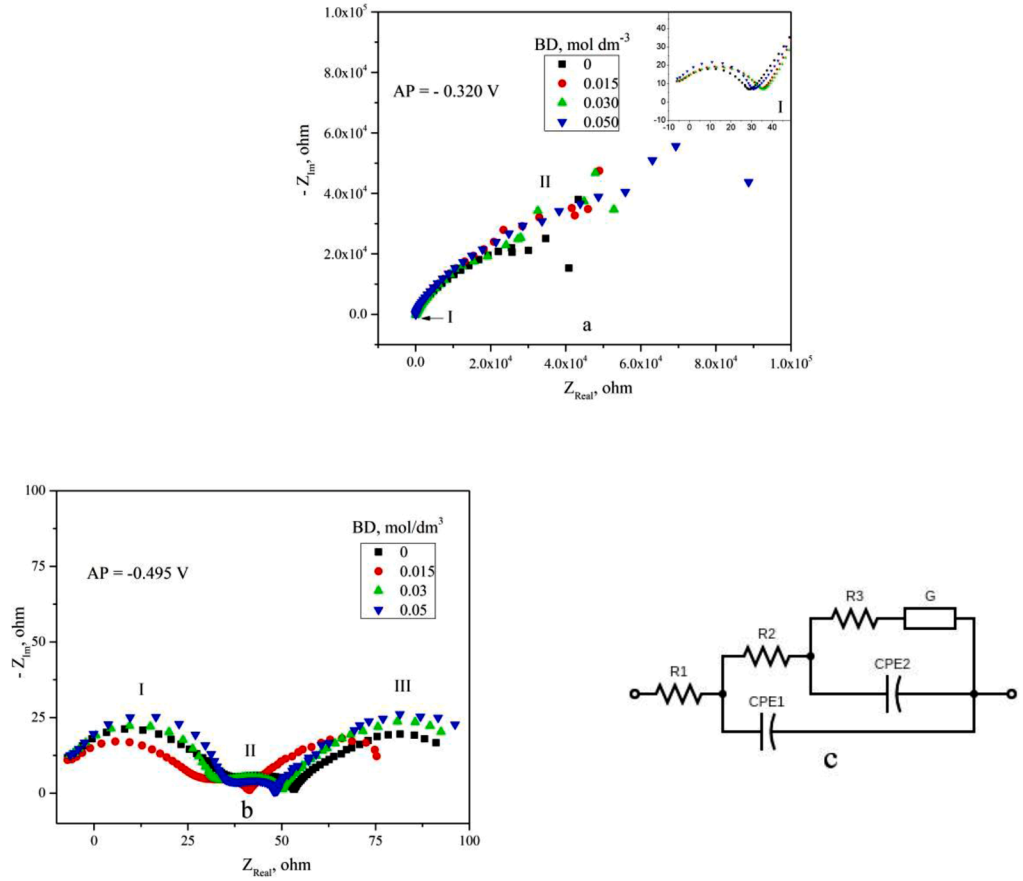

Fig. 9. Nyquist plots for graphite electrode at AP in solution A (a) and solution S (b) with different BD concentration; c – equivalent circuit proposed for solution S modeling.

Table 4
Analyzed electrochemical model impedance parameters from Bode plots of graphite electrode in solution S at –0.495 V.

BD concentration, mol dm^{-3}	0	0.015	0.030	0.050
R_2, Ω	47.1	41.1	44.0	45.7
R_3, Ω	18.1	13.1	15.7	10.9
$Y_{0,2}$, μS	126	121	93.1	62.1
n_2	0.701	0.713	0.763	0.834
K_a, s^{-1}	0.0636	0.0783	0.0460	0.0431
Y_0, mS	73.6	76.6	70.3	65.5

BD into the electrolyte shifts the potential of hydrogen evolution to the field of more negative potentials. This fact explains the decreased porosity of coatings deposited in the presence of BD. Moreover, BD in concentration 0.015 mol dm^{-3} intensifies Sn(II) reduction as it is found from the comparison of cathodic scans of CV curves (Fig. 7, b) and from the calculation of the electrochemical reaction constant from Gerisher element.

It was found that Ag(I) reduction proceeds under the diffusion control owing to its low concentration and the possible formation of π-complexes with BD. Tin(II) reduction is the electron transfer limited process.

The results of electrochemical impedance study revealed that the 0.015 mol dm^{-3} BD additive decrease solution resistance but the resistance rises with the increase in the BD concentration. We propose that the process of the BD complexation with Ag(I) is intensified in the near cathode layer owing to the BD molecules accumulation. In its turn that provides supplementary difficulties in Ag(I) reduction and causes diminution of its content in the alloy. The results of the experiment indirectly indicate that tin(II) does not form stable complex compounds with BD, and that is why the accumulation of BD molecules in the near electrode layer weakly inhibits the process of its reduction.

3.4. Side processes accompanying the electrochemical synthesis of Sn–Ag alloy

Simultaneous Ag(I) and Sn(II) electrochemical reduction from the SA electrolyte can be accompanied by side redox reactions, such as Ag(I) cementation with tin (reaction 1), oxidation of freshly deposited metals with the dissolved oxygen or hydrogen(I). To reveal these processes and to study the effect of the BD on them, the time dependence of the potential of electrodes covered with silver or tin immersed into the electrolyte was analyzed. The open circuit potential was measured for copper electrodes covered with tin coating 10 μm thick deposited in the absence of silver(I) in the SA electrolyte or with silver coating 10 μm thick deposited from traditional cyanide silver plating solution. These electrodes were treated in the electrolyte in the absence of Sn(II) (Fig. 10).

The open-circuit potential for tin electrode in the electrolyte without Sn(II) and Ag(I) practically does not change with time and changes very little with increasing of BD concentration. The presence of Ag(I) in the solution with tin working electrode leads to a significant change in the

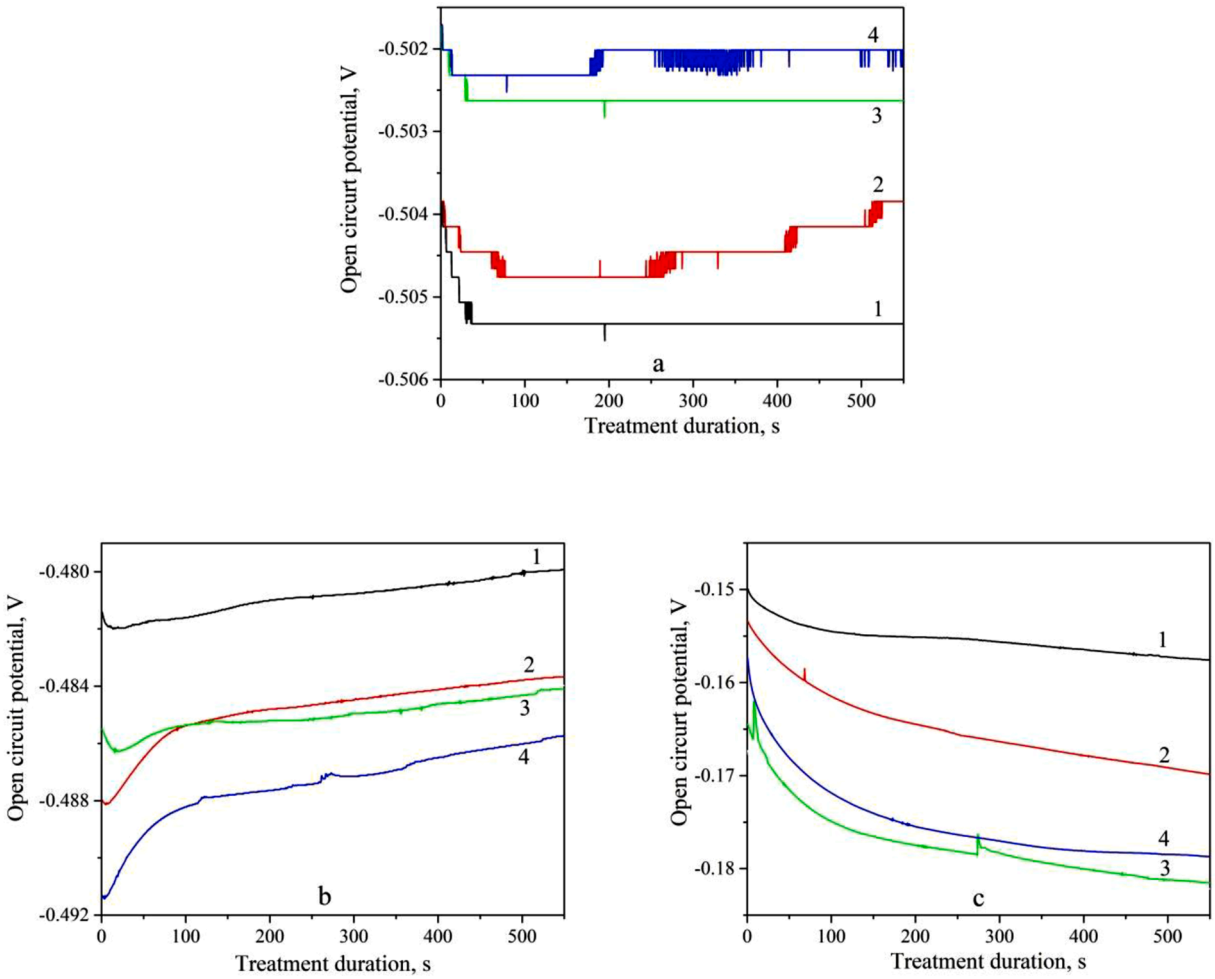

Fig. 10. Time dependence of the open circuit potential: for electrode with tin coatings immersed in the SA solution in the absence of Sn(II) and Ag(I) (a); for electrodes with tin (b) and silver (c) coatings immersed in the SA solution in the absence of Sn(II). Concentration of the BD, mol dm^{-3}: 1 – 0, 2 – 0.005, 3 – 0.015, 4 – 0.030.

electrode potential over time (Fig 10, b). Open circuit potential of tin electrode slightly diminishes for 1−2 mV during the first 10 s after the immersion into the SA electrolyte in the absence of Sn(II) (Fig. 10, b). The value of the potential noticeably depends on the concentration of the BD in the solution decreasing from −0.481 V to –0.491 V. During further treatment of the electrode in the solution the potential increases and after 600 s it reaches −(0.480–0.486) mV. In all cases the value of potential diminishes at the addition of the BD. The decrease in potential during the first seconds of the treatment (Fig. 10, b) can be associated with the reaction 1. Further increase in the potential can be attributed to the adsorption of tin(II) hydroxycompounds appeared in the result of hydrolysis.

Open circuit potential of silver electrode gradually decreases from −0.150 V to −0.157 V with the duration of the treatment in the SA solutions in the absence of Sn(II) and BD. The value of silver electrode potential in the BD availability is more negative (Fig. 10, c), and a decrease in its value with the growth of the treatment duration is more noticeable. The value of this decrease depends on the BD concentration. The shift of the potential to the region of more negative values can be explained by silver corrosion as a result of silver(I) complexation with the Tu resulting in $Ag[Tu]_2^+$, $Ag[Tu]_3^+$ complex compounds formation [17]. The fact of more significant decrease of the potential in solutions with the BD additive, probably, is due to the formation Ag(I) complexes with Tu and BD or mixed complexes.

In the process of electrodeposition partial dissolution of the forming alloy coating or so called “corrosive dissolution of the cathode” is possible. In the previous section, it was found that the presence of BD in the solution causes changes in the composition of the Helmholtz layer. It is likely that BD also affects the rate of corrosive dissolution of the Sn–Ag coating. To test this assumption, the Tafel analysis of curves (linear sweep voltammetry) was carried out for electrodes with tin, silver coatings, as well as with Sn–Ag alloy coating 10 μm thick. The electrodes were immersed into the background solution in the absence of Sn(II) and Ag(I) containing BD in varying concentrations (Fig. 11).

Tafel analysis was carried out with the help of Nova 2.1 software. The Fig. 11 shows the curves linear sweep voltammetry in semi-logarithmic coordinates. Cathodic branches on each curve correspond to hydrogen evolution (reaction 2). Anodic branches show metals oxidation (reaction 9 for Fig. 11, a; reaction 8 for Fig. 11, b). Using Tafel extrapolation method corrosion potentials (E_{corr}) for Sn, Ag, and Sn-Ag coatings were defined. For tin coatings E_{corr} in the examined solutions equals to −0.52 V. Cathodic Tafel slopes for it is −0.049 V dec^{-1} for solution without addition and changes to −0.045 V dec^{-1}. Anodic slope for solution without BD is 0.053 V dec^{-1} and changes to 0.043 V dec^{-1} with BD introduction. Corrosion of tin is slowed down in the presence of BD almost twice due to the raise in overpotential value of hydrogen evolution and anodic dissolution of tin. Corrosion potential for silver coatings in the absence of BD is −0.19 V; minimal quantity of BD shifts E_{corr} to −0.35 V. Following increase in additive concentration slightly raises E_{corr} for silver. Silver dissolution may occur owing to its oxidation with the dissolved oxygen with the formation of complex compound with BD or mixed complex compounds with Tu and BD. Cathodic Tafel slope is −0.11 V dec^{-1}, it does not depend on the BD concentration. Anodic shift value rises with the BD concentration elevating from 0.07 to 0.10 V dec^{-1}. There are no changes in Sn-Ag alloy corrosion potential (−0.51 V). Cathodic and anodic Tafel shifts are −0.12 and 0.05 V dec^{-1} and do not depend on the BD concentration. Alloy corrosion current value is at least twice higher than that for tin in solution with or without BD. Thus, the formation of tin-silver galvanic couple intensifies tin corrosion, owing to the contact of tin with a noble metal. In the BD

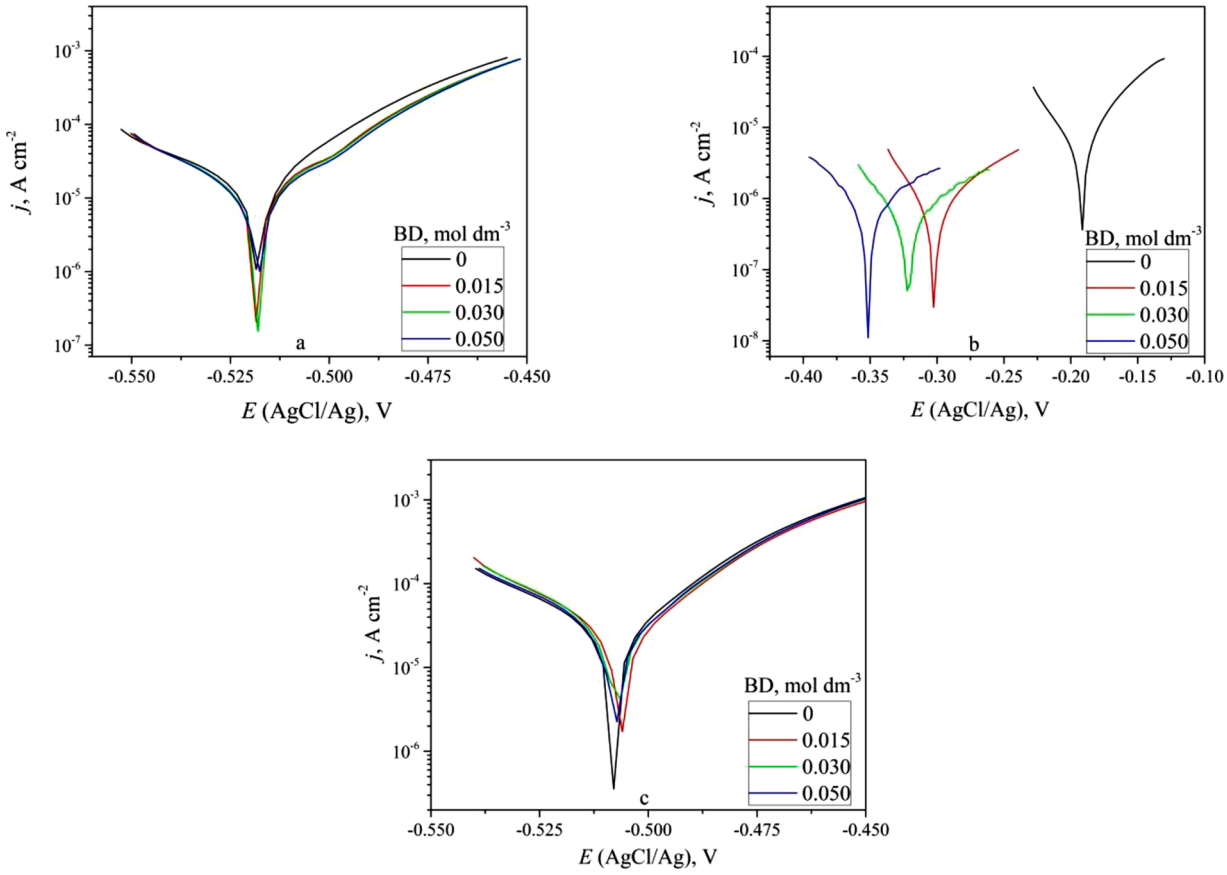

Fig. 11. Potentiodynamic polarization curves illustrating the behavior of electrodes with tin (a), silver (b), Sn-Ag (c) coatings in the SA solution without Sn(II) and Ag(I).

presence in the electrolyte the process of alloy corrosion is slightly retarded.

The study of the BD effect on the side processes accompanying Sn(II) and Ag(I) reduction has shown that tin corrosion in the presence of BD is slowed down but silver corrosion is slightly intensified.

4. Conclusions

The introduction of BD into the solution for the electrochemical deposition of Sn–Ag coatings provides the formation of alloy coatings with the silver content reduced to 7.7–8.1 at.%. Coatings obtained in the presence of BD are close in composition to the eutectic. They consist of two crystalline phases β-Sn and Ag_3Sn. They begin to melt at 221 °C and are more close-packed and low-porous as compared with those obtained in the BD absence. The solution with the BD additive is stable within 3–4 months.

The presence of SnO and SnO_2 oxides and the increased silver content in the near-surface zone of the coatings not more than 2–3 nm deep are distinctive features of the deposited Sn–Ag alloy coatings. These features are due to the occurrence of side processes of Ag(I) reduction with tin and the alloy corrosion, which accompany simultaneous Sn(II) and Ag(I) reduction. Side processes are i) corrosion dissolution of tin in the acid media, ii) Ag(I) reduction by tin in the coating (cementation), iii) hydrogen evolution reaction.

The BD in the electrolyte inhibit the electroreduction of Ag(I) but retards corrosive dissolution of the alloy and hydrogen evolution that provides a decreased porosity of coatings.

Funding

This work was supported by the State Belarusian Program of Scientific Research 4 «Mechanics, Metallurgy, Diagnostics in Mechanical Engineering» subprogram 4.4 «Electroplating», project № 4.1.22.

CRediT authorship contribution statement

M.A. Shikun: Methodology, Investigation, Validation, Formal analysis, Data curtion, Visualization, Writing – original draft. **O.N. Vrublevskaya:** Conceptualization, Methodology, Supervision, Resources, Writing – review & editing. **T.N. Vorobyova:** Conceptualization, Resources, Writing – review & editing, Funding acquisition.

Declaration of Competing Interest

The authors declare that they have no known competing financial interests or personal relationships that could have appeared to influence the work reported in this paper.

Supplementary materials

Supplementary material associated with this article can be found, in the online version, at doi:10.1016/j.surfin.2021.101059.

References

[1] I. Shohji, T. Yoshida, T. Takahashi, S. Hioki, Tensile properties of Sn-3.5 Ag and Sn-3.5Ag-0.75Cu lead free solders, Mater. Trans. 43 (8) (2002) 1854–1875, https://doi.org/10.2320/matertrans.43.1854.

[2] H. Zhang, W.M. Tang, G.Q. Xu, Y.C. Wu, Z.X. Zheng, Synthesis of Sn–Ag binary alloy powders by mechanical alloying, Mater. Chem. Phys. 122 (2010) 64–68, https://doi.org/10.1016/j.matchemphys.2010.02.075.

[3] B. Zhao, W. Zhang, C. Zou, Q. Zhai, S.F.A. Acquah, Y. Gao, Low melting point nanocrystalline Sn–Ag solder synthesized by a refined chemical reduction method, Chin. Sci. Bull. 59 (2014) 4147–4151, https://doi.org/10.1007/s11434-014-0528-7.

[4] H. Jiang, K.S. Moon, C.P.Wong F.Hua, Synthesis and thermal and wetting properties of tin/silver alloy nanoparticles for low melting point lead-free solders, Chem. Mater. 19 (2007) 4482–4485, https://doi.org/10.1021/cm0709976.

[5] O.N. Vrublevskaya, T.N. Vorobyova, M.G. Galuza, M.A. Shikun, A.A. Kudaka, E. E. Venhlinskaya, Synthesis of Powders and Coatings of Tin and Its Alloys with a Controlled Composition and Structure by Cementation from Solutions, Adv. Chem. Res. 52 (2019) 133–252. ISBN: 978-1-53615-314-9.

[6] J. Kim, C.C. Lee, Fluxless Sn–Ag bonding in vacuum using electroplated layers, Mater. Sci. Eng. A. 448 (2007) 345–350, https://doi.org/10.1016/j.msea.2006.10.160.

[7] P. Rossi, N. Zotov, E.J. Mittemeijer, Effects of deposition method on the microstructure and intermetallic compound formation in Ag–Sn bilayers, Surf. Coat. Tech. 295 (2016) 88–92, https://doi.org/10.1016/j.surfcoat.2015.10.057.

[8] M. Bigas, E. Cabruja, Characterization of electroplated Sn/Ag solder bumps, Microelectron. J. 37 (2006) 308–316, https://doi.org/10.1016/j.mejo.2005.05.017.

[9] J.Y. Kim, J. Yu, J.H. Lee, T.Y. Lee, The effects of electroplating parameters on the composition and morphology of Sn-Ag solder, J. Electron. Mater. 33 (2004) 1459–1464, https://doi.org/10.1007/s11664-004-0087-9.

[10] H. Nakano, S. Oue, M. Uranaka, M. Masuda, H. Fukushima, Y. Saka, S. Sawada, Y. Hattori, Electrodeposition of Sn–Ag alloys and evaluation of connection reliability for automotive connector, Mater. Trans. 51 (2010) 712–719, https://doi.org/10.2320/matertrans.M2009425.

[11] M.S. Park, D.H. Nam, K.M. Jung, K.S. Hong, H.S. Kwon, Effects of the degradation of methane sulfonic acid electrolyte on the collapse failure of Sn-Ag alloy solders for flip-chip interconnections, RSC Adv 7 (2017) 23136–23142, https://doi.org/10.1039/C7RA02193C.

[12] A. Gyozova, I. Krastev, L. Petkov, T. Dobrovolska, Electrodeposition and structure of binary alloys of silver, tin and antimony, Bulg. Chem. Commun. Special. Is. B. 48 (2016) 103–109.

[13] Y. Fujiwara, H. Enomoto, T. Nagao, H. Hoshika, Composite plating of Sn–Ag alloys for Pb-free soldering, Surf. Coat. Tech. 169 (2003) 100–103, https://doi.org/10.1016/S0257-8972(03)00169-5.

[14] A. Hrussanova, I. Krastev, G. Beck, A. Zielonka, Properties of silver-tin alloys obtained from pyrophosphate-cyanide electrolytes containing EDTA salts, J. Appl. Electrochem. 40 (2010) 2145–2151, https://doi.org/10.1007/s10800-010-0196-5.

[15] V. Sudha, M. Sangrayanan, Underpotential deposition of metals – progress and prospects in modeling, J. Chem. Sci. 117 (2005) 207–218, https://doi.org/10.1007/BF02709289.

[16] F.C. Walsh, C.T.J. Low, A review of developments in the electrodeposition of tin, Surf. Coat. Tech. 288 (2016) 79–94, https://doi.org/10.1016/j.surfcoat.2015.12.081.

[17] S. Krzewska, H. Podsiadly, Complex of Ag(I) with ligands containing sulfur donor atoms, Polyhedron 5 (1986) 937–944, https://doi.org/10.1016/S0277-5387(00)80133-3.

[18] M. Pettine, F.J. Millero, G. Macchi, Hydrolysis of tin(II) in aqueous solutions, Anal. Chem. 53 (1981) 1039–1043, https://doi.org/10.1021/ac00230a027.

[19] L.X. Wei, A.S.M.A. Haseeb, G. Yingxin, Effects of thiourea and gelatin on the electrodeposition of Sn-Ag solder alloy, in: 4th Asia Symposium on Quality Electronic Design (ASQED), 2012, pp. 291–296, https://doi.org/10.1109/acqed.2012.6320518.

[20] S. Bakkali, R. Touir, M. Cherkaoui, M.Ebn Touhami, Influence of S-dodecylmercaptobenzimidazole as organic additive on electrodeposition of tin, Surf. Coat. Techn. 261 (2015) 337–343, https://doi.org/10.1016/j.surfcoat.2014.11.003.

[21] L. Junfeng, A. Maozhong, Z. Huanyu, Effect of 2-butyne-1, 4-diol on silver electrodeposition from 5, 5-dimethyl hydantoin solutions, Rare Metals 25 (2006) 255–259, https://doi.org/10.1016/S1001-0521(08)60093-5.

[22] B.M. Mykhalichko, Y.I. Slyvka, V.N. Davydov, Copper (I) π-Complexes with Alkyne Ligands: synthesis and Crystal Structure of $M[CuCl_2(HOCH_2C{=}CCH_2OH)]$ ($M{=}K^+$, NH_4^+), Rus. J. Coordin. Chem. 29 (2003) 737–741, https://doi.org/10.1023/A:1026084419011.

[23] O.N. Vrublevskaya, M.A. Shikun, T.N. Vorobyeva, A.M. Rabenok, A.S. Gunich, S. G. Melnikova, Electrochemical deposition of Sn - Ag alloy suitable as a solder, J. Belarus. State Univ. Chem. 1 (2018) 83–91 (in Russ.).

[24] L.T. Rao, P. Rewatkar, S.K. Dubey, A. Javed, S. Goel, Automated pencil electrode formation platform to realize uniform and reproducible graphite electrodes on paper for microfuidic fuel cells, Sci. Rep. 10 (2020) 11675, https://doi.org/10.1038/s41598-020-68579-x.

[25] R.L. McCreery, Advanced Carbon Electrode Materials for Molecular Electrochemistry, Chem. Rev. 108 (2008) 2646–2687, https://doi.org/10.1021/cr068076m.

[26] J.F. Moulder, W.F. Stickle, P.E. Sobol, K.D. Bomben, Handbook of X-ray Photoelectron Spectroscopy, Perkin-Elmer Corporation, Waltham, 1979.

[27] M. Kwoka, L. Ottaviano, M. Passacantando, S. Santucci, G. Czempik, J. Szuber, XPS study of the surface chemistry of L-CVD SnO_2 thin films after oxidation, Thin Solid Films 490 (2005) 36–42, https://doi.org/10.1016/j.tsf.2005.04.014.

[28] S.Z. Kure-Chu, H. Yashiro, Corrosion resistance of multilayered Sn/Ag_3Sn films electroplated on Cu alloys for highly reliable automotive connectors, Electrochem. Soc. J. 161 (2014) 441–449, https://doi.org/10.1149/2.0241410jes.

[29] A.M. Ferraria, A.P. Carapeto, A.M. Botelho do Rego, X-ray photoelectron spectroscopy: silver salts revisited, Vacuum 86 (2012) 1988–1991, https://doi.org/10.1016/j.vacuum.2012.05.031.

[30] N. Elgrishi, K.J. Rountree, B.D. McCarthy, E.S. Rountree, T.T. Eisenhart, J. L. Dempsey, A practical beginner's guide to cyclic voltammetry, J. Chem. Educ. 95 (2018) 197–206, https://doi.org/10.1021/acsjchemed.7b00361.

[31] A. Sadkowski, J.P. Diard, On the Fletcher's two-terminal equivalent network of a three-terminal electrochemical cell, Electrochim. Act. 55 (2010) 1907–1911, https://doi.org/10.1016/j.electacta.2009.11.008.

[32] S. Fletcher, The two-terminal equivalent network of a three-terminal electrochemical cell, Electrochem. Commun. 3 (2001) 692–696, https://doi.org/10.1016/S1388-2481(01)00233-8.

[33] M.E. Orazem, B. Tribollet, Time-constant dispersion. Electrochemical Impedance Spectroscopy, Wiley, New-York, 2008, pp. 233–263, https://doi.org/10.1002/9780470381588.ch13.

[34] A. Lasia, Electrochemical Impedance Spectroscopy and Its Applications, Springer, New York, 2014.